Journal of Electrical Engineering, Vol. 75, No. 2, 2024, pp. 113-123

sciendo

PAPERS

Contact measurement of skin temperature using a wearable two-channel PPG optical sensor supplemented by thermometers

Jiří Přibil[1], Anna Přibilová[1], Ivan Frollo

This paper describes realization, basic properties, testing, and experiments with a special prototype of a wearable two-channel photoplethysmography (PPG) sensor supplemented by contact thermometers that maps the skin temperature at the place where the optical part of the sensor touches a measured hand part (typically a wrist and fingers). Preliminary measurement confirms that proposed I2C thermometers have proper stability and precision, so can be successfully used in the developed PPG sensor. The performed main experiments show that the significant increase of temperature was always observed at the place of the worn PPG sensors during the whole measurement. This rise of temperature affects mainly the PPG signal range, thus it has also influence on the quality of the sensed PPG wave. The conclusion formulates the final recommendation about the necessity of at least 5-minute time delay between the PPG sensor placement on the hand and the start of the PPG signal acquisition. While the current measurements were realized in normal laboratory conditions, the whole wearable PPG sensor consists of non-ferromagnetic materials and all parts are fully shielded by aluminum boxes to enable measurement in a low magnetic field environment which, is our final long term research aim.

Keywords: photoplethysmography optical sensor, wearable sensor, PPG wave features, contact skin temperature measurement

1 Introduction

At present, the magnetic resonance imaging (MRI) is an important imaging technique used for investigation of the heart structure and function [1, 2]. In this type of a non-invasive examining device, the pulsating current in the gradient coil system generates mechanical vibration and acoustic noise [3-5]. Such vibration is often accompanied by a local heating effect which can be measured by a contactless method using a thermal imaging camera [6]. Physiological and psychological impacts of the vibration and noise on a person scanned in an MRI device were observed and practically documented in several studies [7]. The current state of a human cardiovascular system can be described using the shape of the peripheral pulse wave of the photo-plethysmography (PPG) signal which reflects changes in the arterial stiffness, the arterial blood pressure (ABP) [8], the heart pulse rate (PR) [9], pulse transmission time (PTT) [10, 11], pulse wave velocity, etc. These biological parameters can be also used for detection of the stress effect [12, 13] from one or multi-channel PPG signals [9, 14, 15]. In correlation with our final long term research aim, we have tried to apply this technique for detection and quantification of the stress level during examination in the MRI device working with the low magnetic field [16, 17].

The quality of the sensed PPG signals and the determined PPG wave features depends on the actual state of the skin at the position of the optical sensor. Human age and gender as well as the skin colour and the temperature of the skin surface can have influence on the PPG signal, too. Our previous solution of wearable PPG sensors does not allow contact temperature measurement during the PPG signal sensing [16, 17]. For precise determination of PPG wave parameters, the current temperature should be measured at the same time as the PPG signal is sensed. From the reactions of the tested persons we know that majority of them gradually felt pressing and contact thermal effect on the finger (wrist) at the position of the optical part of the sensor. While the time duration of the PPG signal sensing was about 1 minute, the total time of wearing the optical sensor was more than 10 minutes that included the initial time for basic manipulation during sensor mounting and other supplementary operations.

Motivation of the current work was to verify the subjective feeling of local warming by practical measurement experiments using a special prototype of the multi-channel wearable PPG sensor with integrated thermometers. To enable proper and safe function in the weak magnetic field environment of the MRI device, the whole wearable PPG sensor must consist of non-

[1] Institute of Measurement Science, Slovak Academy of Sciences, Bratislava, Slovakia
{umerprib, umerapri, umerollo}@savba.sk

https://doi.org/10.2478/jee-2024-0015, Print (till 2015) ISSN 1335-3632, On-line ISSN 1339-309X

ferromagnetic materials and all parts must be fully shielded by aluminum boxes against the radiofrequency disturbance. Next, we tried to formulate a recommendation about a proper arrangement and timing of PPG signal sensing to obtain clean PPG wave with a sufficient accuracy.

The current article is practically an extension of our previous work [18] – it describes realization, basic properties, process of testing, and experiments performed with a special prototype of a multi-channel wearable PPG sensor. This sensor also contains the contact thermometer to carry out a detailed measurement of the skin temperature at the places where the optical part of the PPG sensor touches a wrist and fingers. The described experiments were realized in the normal laboratory conditions with planned further application for measurements inside the running low-field MRI device [16, 17]. The received data sequences (of two-channel PPG signals and temperature values) were next processed and analyzed statistically. The obtained partial and summary results for all tested persons are presented separately depending on the type of the processed data using graphical as well as numerical forms. The realized measurements confirm continual increase of temperature at the place of worn PPG sensors during the whole experiment. It was caused partially by internal heating from powered analogue parts of optical sensors but mainly by contact warming from the skin of the hand of the tested person. Next, it has been found that the temperature increase depends heavily on the placement of the PPG sensors. Finally, it was detected that the temperature rising has the main influence on the PPG signal range – other parameters seem to be temperature independent or affected by next different factors.

2 Methods

2.1 Determination of PPG wave properties and analysis of sequences of temperature values

For description of signal properties of the sensed PPG waves the energetic, temporal, and statistical parameters can be determined. The methodology currently used for determination of PPG wave properties (including PR) from the PPG wave was described in more detail in [16, 17]. The smoothing and detrending operations must be applied on the sensed raw PPG signal during the pre-processing [19]. Then, the maximum (Lp_{MAX}) and minimum (Lp_{MIN}) levels of the systolic peaks together with the offset level of the PPG signal (L_{OFS}) are determined to obtain the absolute heart pulse range (HP_{RANGE}) as

$$HP_{RANGE} = (Lp_{MAX} + Lp_{MIN})/2 - L_{OFS}. \quad (1)$$

The maximum numerical value of the systolic peak levels and the determined HP_{RANGE} parameter depend on the resolution of the analog-to-digital converter (AD_{RES}) currently used for digitization of an analog signal from a PPG optical sensor. Next, the modulation (ripple) of heart pulses in percentage is calculated as

$$HP_{RIPP} = (Lp_{MAX} - Lp_{MIN}) / Lp_{MAX} \times 100 \quad (2)$$

The PR determination procedure is based on the localized systolic peak positions P_{SYS} in the PPG signal and the determined cycle periods T_{CP}. Using the sampling frequency f_s in Hz, the PR values in min^{-1} are calculated as $PR = 60 \times f_s / T_{CP}$ (see Fig. 1). Subsequently the variance of PR values (PR_{VAR}) is calculated as the squared standard deviation (σ^2).

Distances between localized P_{SYS} positions in samples (ΔP_{SYS}) can be determined from two-channel PPG signals (containing PPG_A, PPG_B waves taken in parallel by sensors located at a known distance [10], [11]). The pulse transmission time (PTT) in ms can be calculated from ΔP_{SYS} value in samples and f_s in kHz as $PTT = \Delta P_{SYS} / f_s$ – see Fig. 2. These values are next applicable for calculation of relative percentage parameter rPTT that is invariant to the current PR value

$$rPTT = (PTT / T_{CP}) \times 100\ (\%). \quad (3)$$

The accuracy of the values produced by the tested temperature sensor (TMP_{SENS}) can be specified by the comparison measurement with a laboratory thermometer (TMP_{LABT}). The data sequences obtained from the measured temperature values (*TMP)* usually include an increasing/decreasing trend which must be removed before their practical usage. For this reason, the linear trend (LT) is calculated by least squares fitting technique of linear regression. After the LT removal, the detrended temperature sequence *TMP'* is ready for the next analysis – see an example in Fig. 3. For comparison of statistical properties of data sequences produced by both evaluated temperature sensors, it is useful to apply the relative variability parameter TMP_{RVAR} calculated as a ratio between the mean and std values of *TMP'* data sequences

$$TMP_{RVAR} = (\sigma\ TMP' / \mu\ TMP') \times 100\ (\%). \quad (4)$$

The temperature changes are determined during the phases of the measurement experiment (with the time duration t_{DUR}) as a difference between T values obtained at the start (T_{START}) and at the end (T_{END}) of the measurement. During the current experiments using the two-channel PPG sensor with two integrated thermometers we have obtained sequences of $T1$, $T2$ temperature values measured in parallel. From these measured temperature sequences, the linear trend parameters (T_{LT}) and relative variation (T_{RVAR}) can be also calculated. Determined positive values of T_{LT} parameters document the raising temperature trend; the negative values represent the falling trend. In addition, it is useful to determine the parameter ΔT_{12} representing differences between T1 and T2 values at T_{END} positions. Thus, in the final numerical comparison, the temperature features of $T_{FEAT} = T_{RVAR}$, T_{LT}, and $\Delta T_{12}\}$ were used. In the case of PPG wave signal properties and heart pulse transmission parameters (PPG_{HPTP}), the parameters such as PR_{RVAR}, HP_{RANGE}, HP_{RIPP}, PTT, and $rPTT$ were used for partial results comparison separately for each PPG wave.

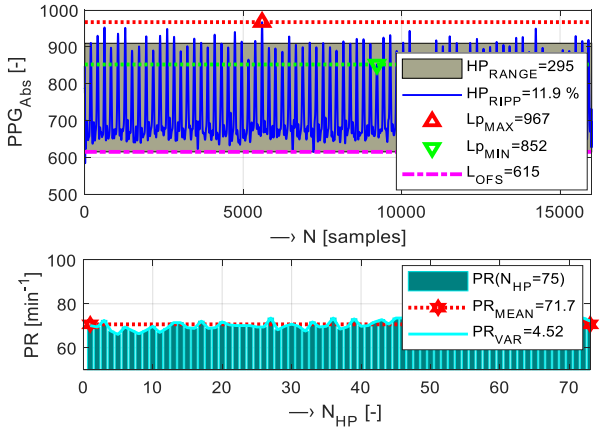

Fig. 1. Example of determination of temporal PPG parameters: 15-k sample two-channel PPG signal (PPG_A wave) with determined Lp_{MAX}, Lp_{MIN}, and L_{OFS} values together with HP_{RANGE} and heart ripple parameters (upper), PR values corresponding to pulse periods T_{HP} ($N_{HP} = 70$) and a mean and variation of PR (lower)

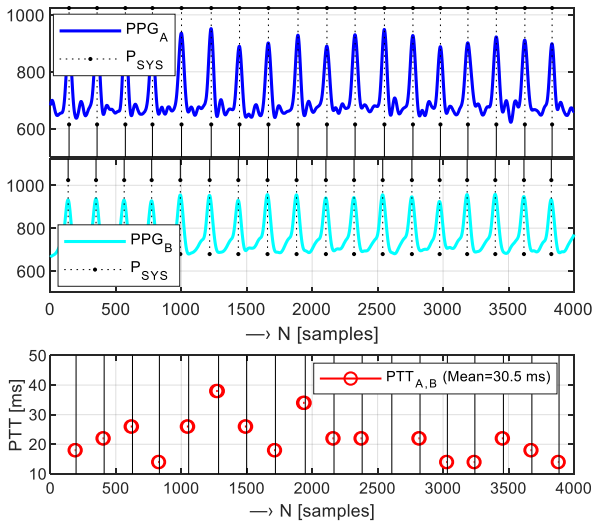

Fig. 2. Example of determination of heart pulse transmission times: visualization of P_{SYS} positions of 4-k sample parts of PPG_A and PPG_B waves (upper set of two graphs), determined PTT values with their mean value; f_s=250 Hz (lower single graph)

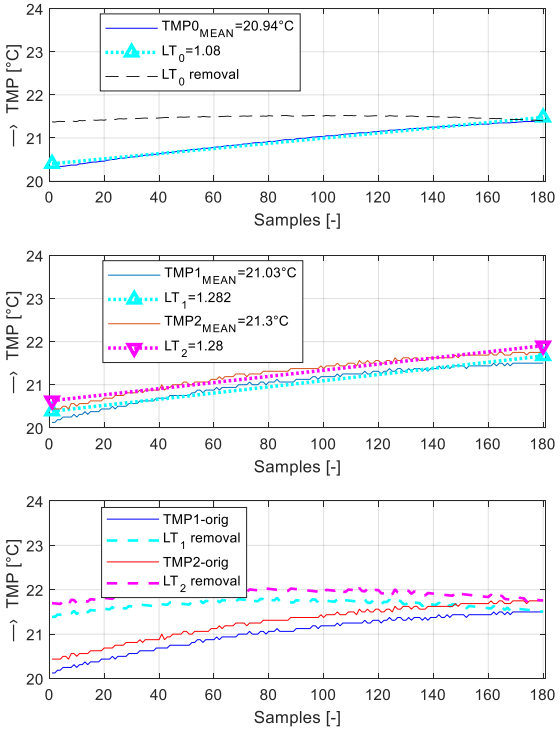

Fig. 3. Example of a linear trend determination and removal of measured temperature data: for data from the laboratory thermometer GMH 3750 (upper graph), measured data from two thermo-sensors MCP9808 together with calculated mean and LT values (middle), original data and detrended temperature sequences *TMP1*', *TMP2*' after LT removal (lower)

3 Objects, experiments and results

3.1 Description of the two-channel wearable PPG sensor with an integrated thermometer

Principally, the multi-channel wearable PPG sensor with an integrated thermometer consists of five basic functional parts as documented in a structure diagram in Fig. 4: (1) optical sensor for PPG signal pickup with analogue interface for raw PPG signal pre-processing and filtering, (2) integrated thermo-sensor using I2C standard, (3) micro-controller with a multi-channel A/D converter and an USB interface, (4) wireless Bluetooth (BT) communication module, (5) power supply using rechargeable batteries or power banks. The currently realized prototype of a two-channel wearable PPG sensor (further called as "PPG-4Tp") represents a relatively simple and low-cost solution, practically consisting of:

- the micro-controller board Adafruit Metro Mini 328 based on the processor ATmega328P, working at f_{CLK} = 16 MHz with eight 10-bit A/D converters, including also a hardware SPI port, a hardware I2C port, and a hardware UART to USB [20],
- the bi-directional communication BT module MLT-BT05, working in the BT4.1 BLE standard at 2.4 GHz,
- two optical PPG sensors working in a reflectance mode with fully integrated analogue interfaces – the Crowtail-Pulse Sensor (ER-CT010712P) – further called as "OS1", and the Gravity Heart Rate Sensor (SEN0203) [21] (next called as "OS2"),
- two integrated high precision I2C thermometers ("MCP1", "MCP2") based on Adafruit MCP9808 temperature sensor [22].

In respect to expected long-term measurement experiments, the whole sensor is powered via the USB port by the 5V power bank THAZER (with 2200 mAh capacity). The tested MCP9808 sensor enables temperature measurement in the range from –40°C to +125°C with a typical accuracy of ±0.25°C. It can work with any micro-controller using the standard I2C. Each sensor includes three address pins so up to eight sensors can be connected in parallel to a single I2C bus. Due to the used optical PPG sensors working on a reflection principle, the sensor's photo detector and light source elements are placed on the same side of the skin surface on fingers or a wrist fixed by an elastic/textile ribbon. For proper and safe function in the magnetic field environment, all parts of the PPG sensor are assembled from elements of non-ferromagnetic materials and are fully shielded in aluminum boxes. As the processor ATmega328P contains eight A/D converters with 10-bit resolution ($AD_{RES} = 2^{10}$), the maximum numerical range of PPG signal samples is 0÷1024.

The whole PPG sensor works in a "slave" mode waiting for commands from the control device to start measurement and real-time transmission of PPG signal samples obtained from optical sensors. The Windows application *PPGsens4Tp.exe* (see a screen copy of the user control panel in Fig. 5) was built to control the two-channel PPG signal acquisition, processing, and storage on a master device (PC, laptop, tablet, etc). It enables: (1) real-time monitoring and displaying of PPG signals picked up currently from two optical PPG sensors, (2) continuous real-time two-channel PPG signal measurement with selected sampling frequency f_S = {125, 250, 500, and 1000 Hz} in data blocks of N_{MEAS} = {1k, 4k, 16k, 32k and 64k} 16-bit (two bytes) samples. For bi-directional serial BT communication between the PPG-4Tp sensor and a control device the maximum baud rate of 115200 bps was used.

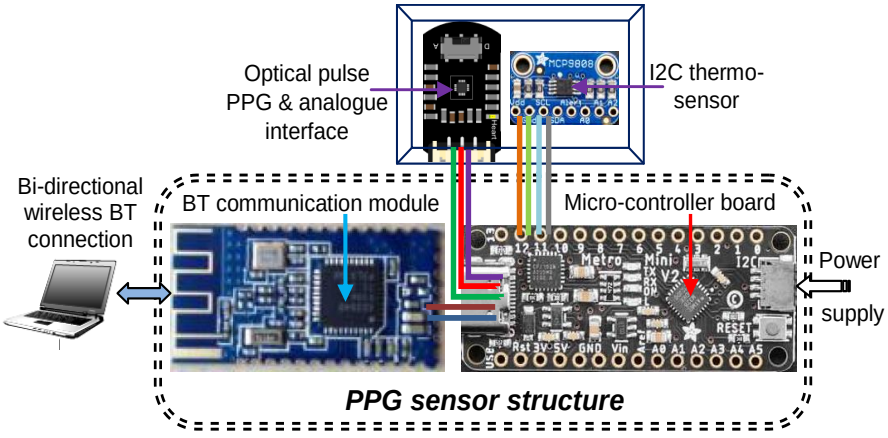

Fig. 4. Principal structure diagram of a wearable PPG sensor with integrated I2C thermometers

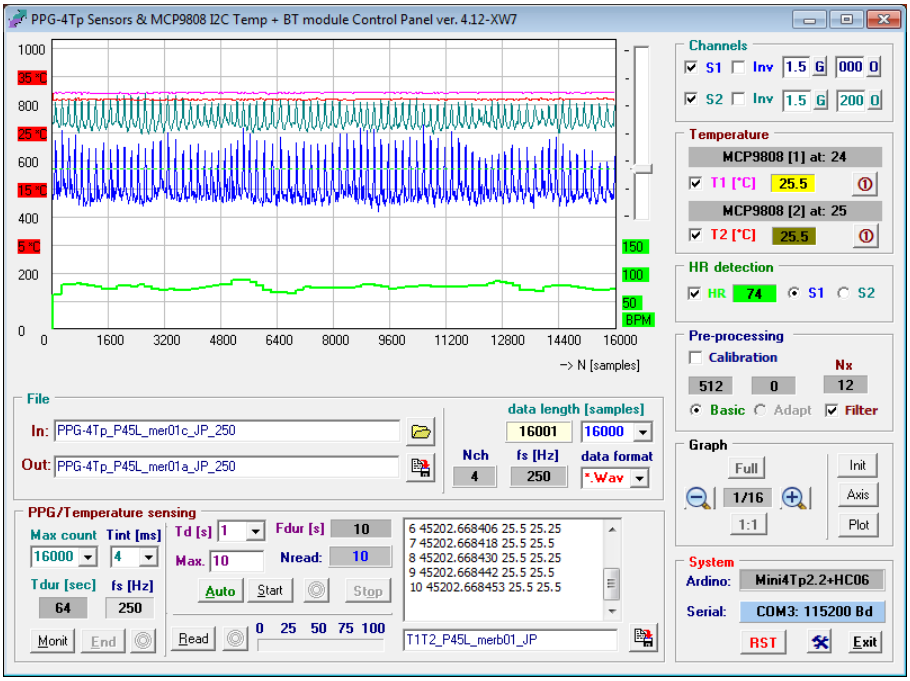

Fig. 5. Screen copy of the control Windows application *PPGsens4Tp*

3.2 Performed analysis, measurements and results

Prior to practical testing and measurement with a developed prototype of the wearable two-channel sensor PPG-4Tp, a short-time as well as a long-term stability and precision of MCP1,2 thermo-sensors were tested in the frame of preliminary experiments. In this stage, parallel measurements inside the temperature stabilized environment of the Minispec pc 100 device with a working static magnetic field of 0.47 T [23] were realized. In these experiments, the high mode resolution of 0.125 °C of MCP9808 sensor chip [22] was set. Both tested thermo-sensors were mounted in parallel at a distance of 5 mm and they have also common wearing for power supply and communication by I2C bus – see a documentary photo in Fig. 6. For comparative measurements, the high-precision thermometer GMH 3750 was used as an etalon [24]. This device consists of the Pt 100 thin film sensor with precision of 0.01 °C and an internal data logger.

At first, we performed three short-time measurements during 3 minutes with temperature sensing in the intervals of T_{INT} = 1 s. Then, we realized three long-term measurements during 3 hours (T_{INT} = 60 s). In both cases, the obtained temperature data records consisted of 180 samples. For evaluation of the short-time comparative measurements, the variability parameter TMP_{RVAR} was finally used.

For analysis of the temperature values from the long-term measurements, differential parameters $TMP1,2_{DIFF}$ were applied. The determined parameters were subsequently statistically processed – see the obtained summary results in Fig. 7.

Fig. 6. Documentary photo of evaluated temperature sensors MCP9808 during comparative measurement by the high-precision thermometer GMH 3750 inside the Minispec pc 100 device

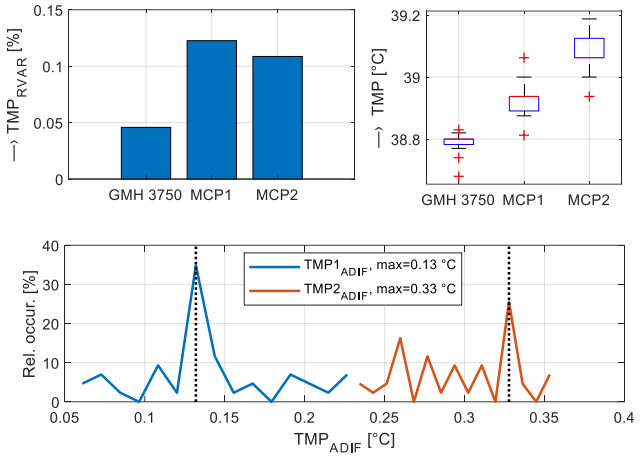

Fig. 7. Summary statistical results of comparative measurements: the bar graph of TMP_{RVAR} values and the boxplot of basic statistical parameters of detrended data sequences *TMP'* after LT removal (upper two graphs), the histogram of TMP_{ADIF} values together with the determined maxima (lower graph)

The integrated thermometers MCP9808 evaluated in this way were next assembled and connected with the optical PPG sensors. After verification of the basic functionality of the whole sensor PPG-4Tp including validation of BT connection with control device (laptop), the main measuring experiment was realized. The principal experiment schedule drawn in Fig. 8 shows that the real-time measurements were practically performed in the following phases:

1. Initialization phase (F0) – optical PPG sensors are mounted on the person's hand; the pressure cuff of a portable BPM device is worn on the arm of the tested person. To eliminate influence of an inflated pressure cuff, the PPG signals must be picked up from the opposite hand. After verification of the PPG signal quality and the presence of the time shift between PPG_A and PPG_B waves for PTT determination, the body of PPG-4Tp sensor is fixed by an elastic ribbon on one arm.
2. Measuring phases F1 and F3 – two-channel PPG signals (waves PPG_A and PPG_B) are recorded together with measured T1, T2 values in a 64-s frame. In parallel, the SBP/DBP and HR values are measured manually using the portable BPM device Microlife BP A150-30 AFIB [25].
3. Measuring phase F2 – in the time duration of 5 minutes, only the T1, T2 values are received from the thermo-sensors MCP1, MCP2 and stored in an output file.

The total time duration of all experiments is about 7 to 10 minutes (depending on the length of the initialization part). In the F0 phase, the first optical PPG sensor OS1 with the thermometer MCP1 is placed on a wrist artery (W), the OS2 sensor with the MCP2 thermometer is worn on the index finger (P4) as demonstrated in an arrangement photo in Fig. 9. The measurements are carried out in normal laboratory conditions. The tested person always sits with both hands laid on the table located in a quiet office room with the mean temperature of about 22°C without any visual, acoustic, or other physical stimuli.

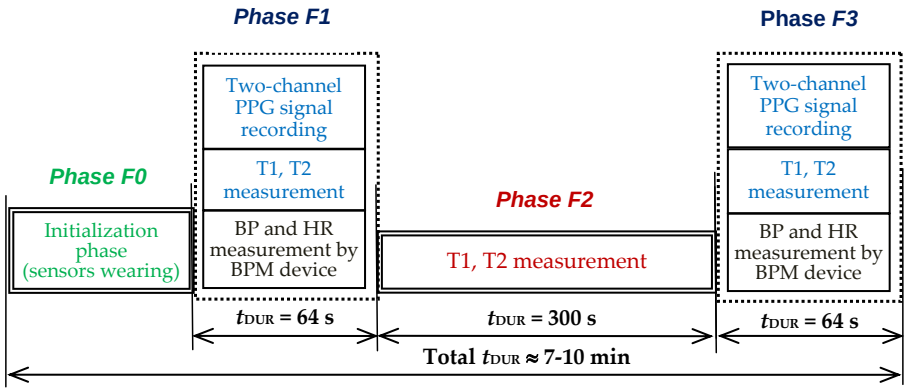

Fig. 8. Principal schedule for PPG signal and temperature values measurement experiments

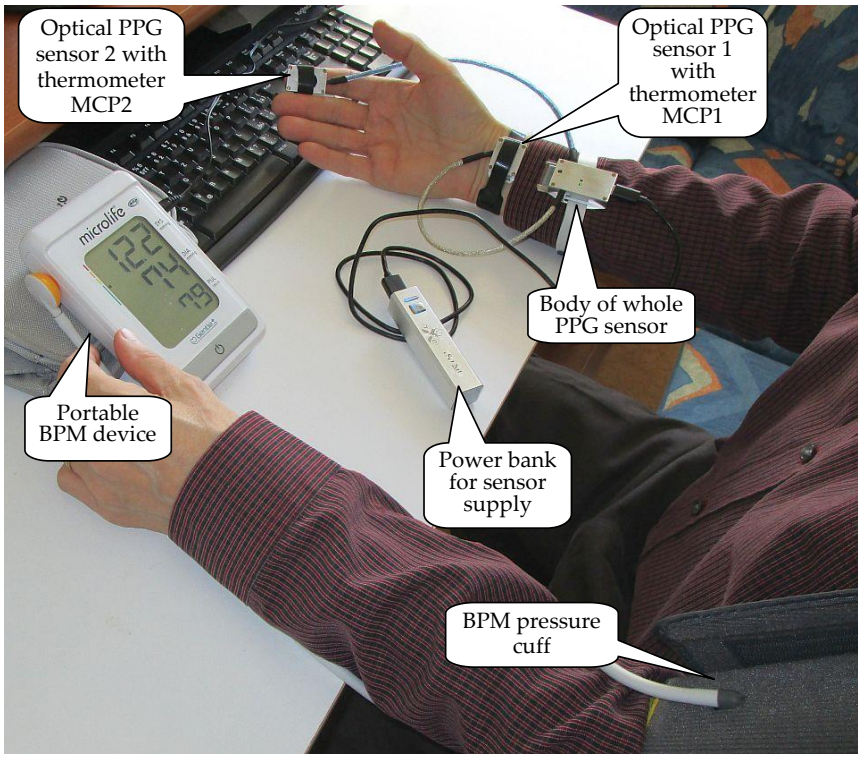

Fig. 9. Photo of experimental arrangement used for PPG and temperature sensing with BP parallel measurement

The sensed PPG signals and measured T1, T2 temperature sequences were collected in a database for further analysis and statistical processing. Each collected database record includes:

1. two PPG wave files containing PPG signals with t_{DUR} = 64 s, sampled at 1 kHz, and T1, T2 sequences sensed in parallel (T_{INT} = 0.2 s) during the F1 and F3 phases,
2. two files with SBP/DBP and HR values measured manually by an external BPM device,
3. one file with temperature T1, T2 values with t_{DUR} = 300 s (T_{INT} = 2 s), measured in the F2 phase.

The data corpus collected in this way consists of records taken from eight volunteer subjects (six males – $S_{M1\text{-}6}$ and two females – $S_{F1\text{-}2}$) with the mean age of 51 years. Partial as well as summary results obtained for all tested persons are evaluated separately depending on the processed signal type:

- Partial results of signal parameters determined from PPG waves taken within the F1 and F3 measure-ment phases for the testing person S_{M1} are shown in Fig. 10. Table 1 enumerates summary mean values of PPG wave temporal features PPG_{TWF} = {*PR*, PR_{RVAR}, HP_{RANGE}, HP_{RIPP}} deter-mined separately for PPG_A and PPG_B waves within the F1, F3 phases for all tested subjects. Table 2 shows calculated differences between PPG_A and PPG_B waves and between the F1 and F3 phases for these parameters ($\Delta PPG_{A\text{-}B}$ F1,3 and $\Delta F1\text{-}F3_{A,B}$). Table 3 compares summary mean values of pulse transmission parameters PPG_{HPTP} ={*PPT*, *rPTT*} in correspondence with systolic/diastolic BP and HR values measured by a BPM device together with enumerated differences between the F1 and F3 phases ($\Delta F1, F3_{HPTP}$).
- The demonstration example of concatenated temperature sequences in the F1, F2, and F3 phases for thermo-sensors MCP1 and MCP2 can be seen in Fig. 11. Numerical comparison of corresponding temperature features T_{FEAT} separately for each measurement phase and final values for the whole measurement (F123) are shown in Table 4. The summary values of T1, T2 temperature features obtained for all tested persons are visualized in graphs in Fig. 12. The boxplot graph shows the basic statistical parameters per the measuring phase and the type of the temperature sequence (T1, T2). Finally, the bar-graphs compare the mean T_{LT} values and the differential ΔT_{12} values.

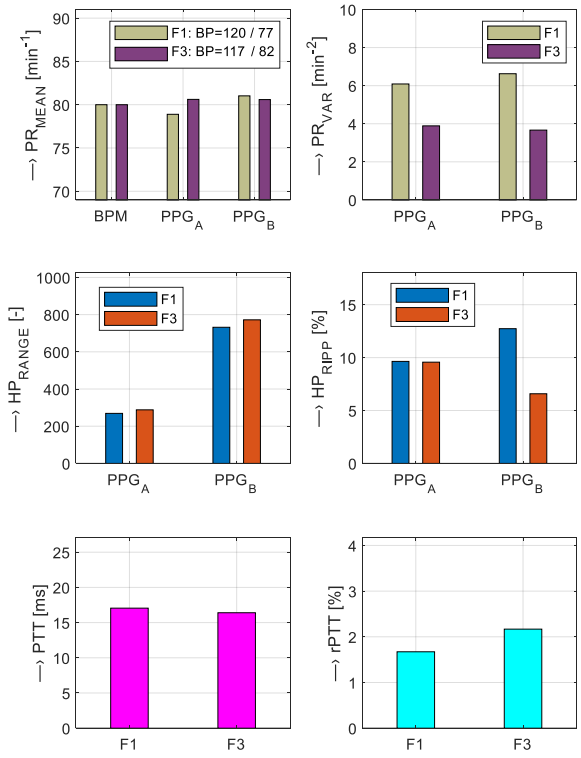

Fig. 10. Partial results of PPG signal properties taken in the F1 and F3 measuring phases: determined mean PR values together with measured BP_{BPM}, HR variations (upper set of bar-graphs), calculated mean HP range and HP ripple values (middle two graphs), PTT and relative PTT values (lower graphs); PPG_A and PPG_B waves sensed at the left hand of the person S_{M4}.

Table 1. Summary mean PPG_{TWF} parameters determined separately for PPG_A and PPG_B waves within the F1 and F3 measuring phases

Measuring phase PPG signal	*PR* (min^{-1})	PR_{VAR} (min^{-2})	HP_{RANGE} (-)	HP_{RIPP} (%)
F1-PPG_A	68.8±7.63	5.2±2.67	227±42	13.4±2.75
F3-PPG_A	70.1±7.68	5.6±4.52	251±52	10.7±3.03
F1-PPG_B	68.2±6.96	5.0±3.49	401±48	9.45±2.33
F3-PPG_B	69.1±7.78	4.7±2.67	459±53	9.34±2.32

Table 2. Calculated differences between the MF1 and MF3 phases of PPG_{TWF} parameters

Difference type	*PR* (min^{-1})	PR_{VAR} (min^{-2})	HP_{RANGE} (-)	HP_{RIPP} (%)
Δ PPG_{A-B} F1	–0.63	–0.21	174	–3.90
Δ PPG_{A-B} F3	–0.98	–0.96	208	–1.32
Δ $F1-F3_A$	1.24	0.39	24	–2.70
Δ $F1-F3_B$	0.89	–0.35	58	–0.12

Table 3. Summary comparison of determined mean PPG_{HPTP} parameters together with measured systolic/diastolic BP and HR values during the F1 and F3 measuring phases

Measuring phase	*SBP* (mm Hg)	*DBP* (mm Hg)	*HR* (min^{-1})	*PTT* (ms)	*rPTT* (%)
F1	122±11	77±6	70±8	17.1±6.4	1.52±0.82
F3	121±14	78±6	70±7	24.6±11.2	2.49±1.12
F3–F1	–1	1	0	7.45	0.97

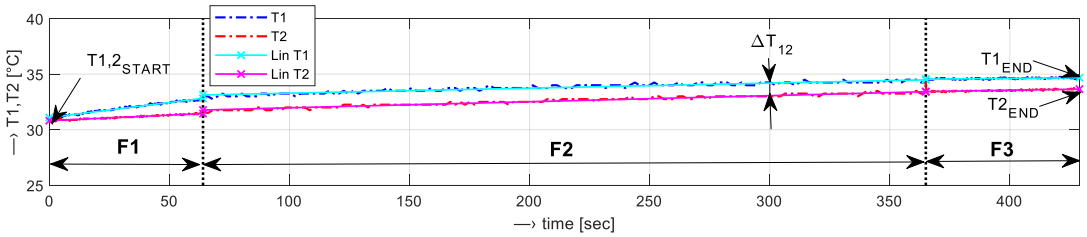

Fig. 11. An example of temperature sequences T1, T2 obtained from sensors MCP1, MCP2 for all three measuring phases (F1, F2, and F3) together with linearization by the calculated LT, t_{DUR}=428 s, the testing person S_{M1}

Table 4. Statistical parameters of T_{FEAT} features determined from T1, T2 temperature sequences given in Fig. 11

Phase / T_{FEAT}	T_{MEAN} (°C)		T_{RVAR} (%)		T_{LT} (°C)		Δ T_{12} [°C]
	T1	T2	T1	T2	T1	T2	
F1[A)]	31.9±0.40	31.1±0.47	0.16	0.22	1.72	0.64	1.12
F2	33.8±0.57	32.6±0.62	0.33	0.39	1.36	1.65	1.07
F3[B)]	35.5±0.42	34.6±0.48	0.18	0.23	0.13	0.22	1.03
F123	33.5±0.49	32.4±0.51	0.24	0.26	–	–	–

[A)] $T1,2_{START}$ = 30.81 °C, [B)] $T1_{END}$= 34.68 °C, $T2_{END}$= 33.65 °C

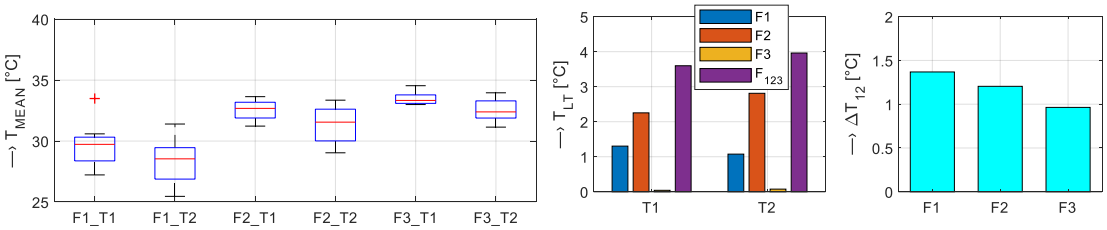

Fig. 12. Graphical comparison of summary values of T1, T2 temperature features obtained for all tested persons (from left to right): boxplot graph of the basic statistical parameters, bar-graphs of mean T_{LT} values, and differential ΔT_{12} values

4 Discussion and conclusion

Preliminary experiments based on a comparative measurement with the high-precision thermometer GMH 3750 inside the temperature stabilized environment show very good short-term as well as long-term stability and proper precision of the used thermo-sensors MCP1,2. The obtained results show that these I2C thermometers based on MCP9808 chip produce temperature values with a relative variance of about 0.13 % which is fully comparable with the used etalon device. Contrary to our expectations, there exist constant differences between MCP1 a MCP2 values – see the bottom histogram in Fig. 7. On the other hand, the detected absolute difference of about 0.2 °C corresponds to a typical certified precision in the normal mode resolution [22]. Hence these currently investigated thermo-sensors could be subsequently assembled and connected with the optical PPG sensors for next measurement experiments and analysis.

The performed main experiments have demonstrated that continually raised temperature during all 7-minute measurements had influence on PPG signals features sensed in the F1 and F3 phases – compare summary mean results of PPG_{TWF} parameters in Table 1 and differential parameters in Table 2. These values are in a good correspondence with the partial graphical

results presented in Fig. 10. Two-channel PPG signals consisting of PPG_A and PPG_B waves taken in parallel in the F3 phase have always higher HP_{RANGE} in comparison with the $PPG_{A,B}$ sensed in the F1 phase. Next, the PPG signal taken from the index finger has slightly lower range in comparison with the second one, taken from the wrist. In the case of the HP_{RIPP} parameter, this trend was not finally confirmed (see the last columns in Tables 1 and 2) – so these values are practically temperature independent. Higher values of the variance of PR (PR_{VAR} parameter) obtained in the F1 phase have direct relationship with lower HP_{RANGE} of the sensed PPG signal. Summary comparison of mean PPG_{HPTP} parameters given in Table 3 shows slight but detectable extension of pulse transmission times in the F3 phase, while the mean values of the measured SBP/DBP and HR parameters values are practically the same – see the last line representing a difference between the F1 and F3 phases. Observed continual increase of T1, T2 temperatures within F1-3 phases (see an example of concatenated T1, T2 sequences in Fig. 11) was caused partially by internal heating from the powered analogue parts of the optical sensors but mainly by contact warming from the skin of the hand (wrist and finger) of the tested person. It was found that the temperature increase depends heavily on the placement of the PPG sensor: the highest T_{LT} was obtained from T1 values measured by the thermo-sensor worn on the wrist while the T_{LT} values determined from T2 sequences are higher in other two measuring phases F2 and F3 – see partial results in Table 4 as well as the final graphical comparison in Fig. 12. On the contrary, the final increase of T2 values taken from the index finger was always lower than T1 ones as also documents the box-plot graph of T1, T2 values for all three measuring phases in Fig. 12. The maximum difference ΔT_{12} between T1 and T2 sequences was detected at the T_{END} position of the F1 phase and it had practically constant character until the end of the whole measurement as can be seen in the right bar-graph of Fig. 12. On the other hand, the F2 phase produces T1, T2 values with slightly higher variability in comparison with other phases as documented by the partial result of an example in Fig. 10 and statistical parameters of temperature features enumerated in Table 4.

The results of the currently performed experiments show that the PPG wave with proper quality and accuracy can be obtained by the optical PPG sensors keeping worn on the tested hand parts (fingers/wrist) at least 5 minutes before the start of the PPG signal sensing. This time delay enables the skin placed under the sensor to adapt, improves blood circulation, and brings the PPG signal with higher absolute range in the final effect.

In the near future, we will try to collect larger database of multi-channel PPG signals, including long-term temperature sequences from measurements in a low magnetic field environment, i.e., inside the scanning MRI device based on up to 0.2 T (open-air/whole-body types located at our institute). In addition, we plan to supplement the measurement experiments by sensing temperature image of the whole hand by a thermal-imaging camera to document differrences before and after examination inside the MRI tomograph.

Acknowledgment

The work has been supported by the Slovak Scientific Grant Agency project VEGA 2/0004/23.

References

[1] K. Fischbach et al. “Cardiac Magnetic Resonance Imaging Using an Open 1.0T MR Platform: A Comparative Study with a 1.5T Tunnel System“, *Pol. J. Radiol.*, vol. 82, pp. 498–505, 2017, https://doi.org/10.12659/PJR.899822

[2] J. Brablik et al, “A comparison of alternative approaches to MR cardiac triggering: A pilot study at 3 Tesla“, *IEEE Journal of Biomedical and Heath Informatics*, vol. 26, no. 6, pp. 2594-2605, 2022. https://doi.org/10.1109/JBHI.2022.3146707

[3] C. K. Mechefske, “Acoustic noise in MRI scanners“. *Biomedical Applications of Vibration and Acoustics in Therapy, Bioeffect and Modeling*. ASME, New York, 2008, pp. 275-328.

[4] Z. Wu, Y. C. Kim, M. C. K Khoo, and K. S. Nayak, “Evaluation of an independent linear model for acoustic noise on a conventional MRI scanner and implications for acoustic noise reduction“, *Magnetic Resonance in Medicine*, vol. 71, pp. 1613-1620, 2014, https://doi.org/10.1002/mrm.24798

[5] E. T. Tan, et al. “Reduced acoustic noise in diffusion tensor imaging on a compact MRI system“, *Magn. Reson. Med.*, vol. 79, pp. 2902–2911, 2017, https://doi.org/10.1002/mrm.26949

[6] A. Glowacz, “Thermographic fault diagnosis of electrical faults of commutator and induction motors“, *Engineering Applications of Artificial Intelligence*, vol. 121, 105962, 2023, https://doi.org/10.1016/jengappai.2023.105962

[7] M. C. Steckner, “A review of MRI acoustic noise and its potential impact on patient and worker health“, *eMagRes*, vol. 9, pp. 21-38, 2020, https://doi.org/10.1002/9780470034590.emrstm1628

[8] C. O. Manlises et al. “Monitoring of Blood Pressure Using Photoplethysmographic (PPG) Sensor with Aromatherapy Diffusion“. In *Proceedings of the 6th IEEE International Conference on Control System, Computing and Engineering*, 25–27 November 2016, Penang, Malaysia, pp.476-480.

[9] M. Nitzan, and Z. Ovadia-Blechman, “Physical and physiological interpretations of the PPG signal“, *Photoplethysmography: Technology, Signal Analysis, and Applications*,., Allen, J., Kyriacou, P.A. Eds.; Elsevier: London, United Kingdom, 2022; pp. 319–339, ISBN: 978-0-12-823374-0, https://doi.org/10.1016/B978-0-12-823374-0.00009-8

[10] M. Zhang, P. F. Wei, and Y. Li, “A LabVIEW based measure system for pulse wave transit time“. In *Proceedings of the International Conference on Information Technology and Applications in Biomedicine,* Shenzhen, China, 30–31 May 2008.

[11] B. M. McCarthy, B. O'Flynn, and A. Mathewson, "An Investigation of Pulse Transit Time as a Non-Invasive Blood Pressure Measurement Method", *Journal of Physics: Conference Series*, vol. 307, 2011, https://doi.org/10.1088/1742-6596/307/1/012060
[12] H. Ahmed, and R.J. Rony, "Understanding self-reported stress among drivers and designing stress monitor using heart rate variability", *Quality and User Experience*, vol. 6, no. 4, 2021, https://doi.org/10.1007/S41233-020-00043-0
[13] P. Celka, P.H. Charlton, B. Farukh, P. Chowienczyk, and J. Alastruey, "Influence of mental stress on the pulse wave features of photoplethysmograms", *Healthc Technol Lett* , vol. 7, pp. 7–12, 2020, https://doi.org/10.1049/htl.2019.0001
[14] M. Abbod, Y-R. Chiou, S-H. Yang, S-Z. Fan, and J-S. Shieh, "Developing a monitoring psychological stress index system via photoplethysmography", *Artif Life Robotics* 16:430–433, 2011, https://doi.org/10.1007/s10015-011-0976-y
[15] L. Wang, B. P. Lo, and G. Z. Yang, "Multichannel reflective PPG earpiece sensor with passive motion cancellation". *IEEE Transactions on Biomedical Circuits and Systems*, vol. 1, no. 4, pp. 235-241, 2007, https://doi.org/10.1109/TBCAS.2007.910900
[16] J. Přibil, A. Přibilová, and I. Frollo, "Physiological impact of vibration and noise in an open-air magnetic resonance imager: Analysis of a PPG signal of an examined person", *Proceedings*, vol. 42, 14. 2020, https://doi.org/10.3390/ecsa-6-06631
[17] J. Přibil, A. Přibilová, and I. Frollo, "First-step PPG signal analysis for evaluation of stress induced during scanning in the open-air MRI device", *Sensors*, vol. 20, 3532, 2020, https://doi.org/10.3390/s20123532
[18] J. Přibil, A. Přibilová, and I. Frollo, "Wearable PPG Optical Sensor with Integrated Thermometer for Contact Measurement of Skin Temperature " in Proceedings of the 10th International Electronic Conference on Sensors and Applications, 15–30 November 2023, MDPI: Basel, Switzerland, https://sciforum.net/paper/view/16249
[19] M. Elgendi, "PPG Signal Analysis: An Introduction Using MATLAB", CRC Press, 27-36, 2021. ISBN 978-1-138-04971-0.
[20] Adafruit Metro Mini 328 V2 - Arduino-Compatible - 5V 16MHz - STEMMA QT / Qwiic. Available online: https://www.adafruit.com/product/2590 (accessed on January 6, 2023)
[21] Gravity: PPG Heart Rate Monitor Sensor for Arduino (Analog/Digital). Available online: https://www.dfrobot.com/product-1540.html (accessed on January 6, 2023)
[22] Adafruit MCP9808 Precision I2C Temperature Sensor Guide. Available online: https://cdnlearn. adafruit.com/downloads/pdf/adafruit-mcp9808-precision-i2c-temperature-sensor-guide.pdf (accessed on January 6, 2023)
[23] P. Andris, et al. "Conversion of the Bruker Minispec Instrumentation into the Static Magnetic Field Standard". Measurement, vol. 23, no. 3, pp. 124-129, 2023, https://doi.org/10.2478/msr-2023-0016
[24] Pt100 – high-precision thermometer, data logger. Available online: https://www.greisinger.de/p/handmessgeraete-undsensoren/temperatur/geraete-pt100/gmh-3750/600335/#googtrans(de|en) (accessed on January 6, 2023).
[25] Microlife BP A150 AFIB. Available online: https://www.microlife.com/support/blood-pressure/bp-a150-afib (accessed on December 12, 2022).

Jiří Přibil was born in 1962 in Prague, Czechoslovakia. He received his MSc degree in computer engineering in 1991 and his PhD degree in applied electronics in 1998 from the Czech Technical University in Prague. At present, he is an independent researcher at the Department of Imaging Methods, Institute of Measurement Science, Slovak Academy of Sciences in Bratislava. At present, he is oriented to analysis of effect of the noise and mechanical vibrations in scanning area of the MRI scanner on the examined person, methods for detection and evaluation of stress effects on the human cardio-vascular system based on photoplethysmographic and speech signals.

Anna Přibilová received her MSc and PhD degrees from the Faculty of Electrical Engineering and Information Technology, Slovak University of Technology (FEEIT SUT) in 1985 and 2002, respectively. In 2014 she has become an associate professor at the Institute of Electronics and Photonics of the FEEIT SUT in Bratislava. At present, she is an independent researcher – scientific worker at the Department of Biomeasurements in the Institute of Measurement Science, Slovak Academy of Sciences in Bratislava. Her research lies in the area of biomedical signal measurement, processing, and analysis.

Ivan Frollo was born in Presov, Slovakia, in 1939. He received his Ing (MSc) degree in 1963 from the Slovak University of Technology, Faculty of Electrical Engineering and his CSc, (PhD) and DrSc in 1967 and 1992, respectively, from the Slovak Academy of Sciences. Since 1995 he has been full professor. His academic orientation is in the field of electrical engineering, signal processing, electronics for hydraulics, medical imaging techniques based on nuclear magnetic resonance. He was with the Institute of Measurement Science, Slovak Academy of Sciences as head of the Department of Imaging Methods and manager of many research projects.

Received 29 January 2024